2020 American Control Conference
Denver, CO, USA, July 1-3, 2020

Investigating the Underlying Dynamical Structure of Supersonic Flows Using Effective Model Reduction

Dan Wilson[1*], Samir Sahyoun[2], Phil Kreth[3], and Seddik M. Djouadi[1]

Abstract— **The temporal features of a cylinder-generated shock-wave/transitional boundary-layer interaction (XSWBLI) in response to supersonic flow (Mach 2) are investigated using various model reduction techniques. Experimental data are obtained using schlieren imaging at 100 kHz and image analysis is performed using proper orthogonal decomposition (POD). The POD framework is used as a starting point to define a reduced set of data-driven isostable coordinates that characterize the transient behavior of an underlying dynamical system. Observed unsteady behaviors in the shock-wave/boundary-layer interactions are well-represented as an externally forced dynamical system with a pair of complex-conjugate isostable coordinates. Results are validated against well-established reduction methodologies including POD and spectral POD. These results indicate that the isostable reduced coordinate framework can be used to provide an accurate, low-dimensional representation of the dynamical features of supersonic fluid flow, even when the relationships between underlying dynamical model and observed output are not explicitly known.**

I. Introduction

Recent years have seen a resurgence of interest in model reduction techniques for extracting low-dimensional representations from high-dimensional models. Among the most well-established reduction methods is proper orthogonal decomposition (POD) [1], [2], [3], which seeks to find an optimal orthogonal basis to characterize observed data; variants include clustering POD [4], spectral POD [5], balanced POD [6], and adaptive POD [7]. Dynamic mode decomposition (DMD) is a more recently developed methodology that can be used to represent the spatiotemporal evolution of a dynamical system using a finite number of basis elements [2], [8]. DMD is closely related to Koopman analysis, a framework that represents the evolution of system observables using an infinite-dimensional, linear operator [9], [10].

A commonality among each of these aforementioned methods is that they try to characterize the underlying dynamical features of high-dimensional experimental data using a reduced order basis. When that data is generated by a dynamical system that is fundamentally nonlinear, the identification of a suitable basis poses significant challenges. POD is able to represent experimental data efficiently, but subsequent extraction of dynamical information is typically difficult. On the other end of the scale, DMD (and related analysis methods using the Koopman operator) can be used to represent the temporal evolution of the observables of a nonlinear system, but in most cases a large number of basis elements is required, limiting the utility of the reduction strategy. Refined methods for the identification of representative observable functions to represent the Koopman eigenfunctions are actively being developed [6], [11], [12].

In this work, we investigate the use of isostable coordinates to define a basis of functions that can be used to represent fluid flow data. In the basin of attraction of a fixed point or stationary solution, these isostable coordinates are directly related to the level sets of the most slowly decaying Koopman modes [13], i.e., they characterize the infinite time convergence of initial conditions to the stationary solution. We apply this framework to experimental data of shock-wave/transitional boundary-layer interaction resulting from Mach 2 flow past a standing cylinder. Shock-wave/boundary-layer interactions (SWBLI) are one of the dominant sources of scientific uncertainty and resultant technical risk in the development of planned hypersonic capabilities for national defense and responsive space access. Although SWBLI have been the subject of significant research for more than 50 years [14], [15], only recently have experimental and computational capabilities become available to effectively resolve and characterize the critical fluid dynamic phenomena that drive their behavior. Characterizing SWBLI that occur with boundary layers undergoing laminar-turbulent transition can be challenging as shock-wave/transitional boundary-layer interactions (XSWBLI) may have significant unsteady components which can be difficult to model and predict. Here, we investigate the application of isostable coordinates on experimental data of an XSWBLI resulting from Mach 2 flow past a standing cylinder. This configuration is an ideal test-bed for the proposed method due to the unsteady behavior of the interaction. Using the isostable reduced framework, we identify a reduced set of dynamical features responsible for the unsteady behavior of the shock structure. The results using the isostable method are compared and validated against more well-established model reduction frameworks.

The organization of this paper is as follows: in Section II we describe the experimental setup used to obtain the fluid flow data. Section III details the isostable coordinate based reduction method and gives related results. Section IV provides comparisons with other well-established reduction frameworks, and Section V gives concluding remarks.

II. Experimental Methods

The experimental data analyzed within the present work were obtained in the Mach 2 low-enthalpy blowdown wind

[1]Department of Electrical Engineering and Computer Science, University of Tennessee, Knoxville, TN 37996, USA
[2]Uppsala University, Uppsala, Sweden
[3]Department of Mechanical, Aerospace, and Biomedical Engineering, University of Tennessee Space Institute, Tullahoma, TN 37388, USA
* dwilso81@utk.edu

tunnel facility at the University of Tennessee Space Institute (UTSI). The wind tunnel test section has a constant cross-section of 203×203 mm, and the plenum pressure is maintained by a control valve at approximately 240 kPa. The freestream velocity is on average 507 m/s, and the freestream Mach and unit Reynolds numbers are 2.01 and approximately 3.0×10^7 m^{-1}, respectively. Optical access for the schlieren imaging is provided by BK7 glass viewports on the wind tunnel side walls.

A Z-type schlieren system was used for flow visualization of the shock interaction. The primary field elements are 2.67-m-focal-length mirrors, and pulsed illumination is provided by a high-powered light-emitting diode (LED). The LED and a Photron FASTCAM Mini UX100 high-speed camera are synchronized at a 100 kHz repetition rate. An exposure of 700 nanoseconds is short enough to effectively freeze the high-speed flow in each image. The resulting images (32×1024 pixels) have a resolution of 6 pixels/mm.

The test model utilizes a 3.2-mm-diameter (d), 12.7-mm-tall (h) cylinder mounted to an inclined (-6.3 deg) flat plate with a sharp leading edge (8 deg). The negative angle of attack prevents flow separation near the leading edge and yields an edge Mach number of approximately 1.78. Experiments were conducted at a variety of cylinder locations relative to the flat plate leading edge, though data presented here are shown for the cylinder placed $7d$ (22.2 mm) downstream of the leading edge. At these locations, the boundary layer on the flat plate is undergoing laminar-turbulent transition, such that a shock-wave/transitional boundary-layer interaction (XSWBLI) is present.

A typical schlieren image of the cylinder-generated XSWBLI is shown in Panel A of Figure 1. Here, the flow is from left-to-right, the flat plate is at the bottom edge of the image, and the cylinder is on the right. The various flow features associated with this interaction are shown in the schematic in Panel B. The relevant features of interest to the present study are the forward shock foot, upstream influence, flow separation region, and inviscid shock. Further details on the experiments and the fluid dynamics analyses are presented in [16].

III. Image Analysis of Experimental Data Based on Isostable Coordinates

The notion of isostable coordinates has been used to characterize the transient decay of solutions to an attractor of a nonlinear dynamical system, [13], [17], [18]. When the attractor is a fixed point, these isostable coordinates are directly related to level sets of a particular mode of the Koopman operator [13]. In these instances, isostable coordinates can be computed by comparing the infinite time behavior of solutions within the basin of attraction of a limit cycle to the eigenfunctions associated with the linearized fixed point. When working with low-dimensional or numerical simulations, it is relatively straightforward to compute the required eigenfunctions and associated eigenvalues. When working with high-dimensional systems or with experimental data, direct computation of eigenvalues and eigenfunctions

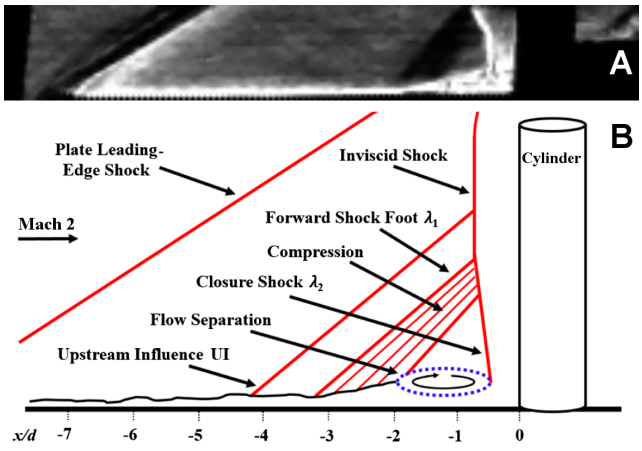

Fig. 1. Cylinder-generated shock-wave transitional boundary-layer interaction (XSWBLI). The schematic is reproduced from [16].

is impractical. The authors of [19] propose one method for inference of eigenfunctions if the associated eigenvalues are known *a priori*. Here we describe a different approach that can be implemented without explicit knowledge of these eigenvalues.

Consider a general PDE on the domain Ω,

$$\begin{aligned} \frac{\partial}{\partial t}X(r,t) &= F(X(r,t)) + G(X(r,t)), \\ Y(r,t) &= C(X(r,t)), \end{aligned} \tag{1}$$

with boundary conditions

$$X(r,t) = b_{\text{nom}}(r) + b_{\text{t}}(r,t) \text{ for } r \in \partial\Omega. \tag{2}$$

Here, $X(r,t)$ represents the state as a function of location, r, and time, t, $Y(r,t)$ is a measured observable, C a linear function of the state, local dynamics are given by F, spatial coupling is represented by G (e.g., advection and diffusion in the case of the Navier-Stokes equation), $b_{\text{nom}}(r)$ gives the nominal Dirichlet boundary conditions and $b_{\text{t}}(r,t)$ accounts for temporal fluctuations, for instance, to characterize statistical fluctuations observed in an experiment. We will take the mean value of $b_{\text{t}}(r,t)$ to be zero for all r which can always be accomplished with an appropriate choice of $b_{\text{nom}}(r)$. In the derivation to follow, we assume the $b_{\text{t}}(r,t) = 0$, but will lift this restriction as part of the experimental imaging analysis. As in [20], we assume that when $b_{\text{t}}(r,t) = 0$, Equation (1) has a stationary solution $X_{\text{SS}}(r)$ for which $F(X_{SS}(r)) + G(X_{SS}(r)) = 0$. We also assume that the operator $J \equiv \nabla[F(X_{SS}(r)) + G(X_{SS}(r))]$ (i.e., the local linearization with respect to the stationary solution) exists and is compact. As illustrated in [19], near X_{SS}, a leading order accurate solution to the PDE can be written using a basis of eigenfunctions $\rho_j(r)$ of J with corresponding eigenvalues λ_j:

$$X(r,t) - X_{\text{SS}}(r) = \sum_{j=1}^{\infty} s_j \left[X(r,0) - X_{\text{SS}}(r)\right] \rho_j(r) e^{\lambda_j t}, \tag{3}$$

where $s_j(x)$ give the coordinates of X in the eigenfunction basis, and $X(r,0)$ is an initial state. Let the eigenvalues be

sorted so that $0 \geq \mathrm{Re}(\lambda_j) \geq \mathrm{Re}(\lambda_{j+1})$, i.e., with λ_1 corresponding to the eigenfunction with the slowest rate of decay. For the slowest decaying eigenfunctions, an eigenfunction basis can be used to define isostable coordinates according to [20]

$$\psi_j\{X(r)\} = \lim_{t\to\infty} e^{-\lambda_j t}\int_\Omega Q_j^T(r)(X(r,t)-X_{SS})dr, \quad (4)$$

where $Q_j(r)$ is used to to project the solution onto $\rho_j(r)$ and is defined so that $\int_\Omega Q_j^T(r)\rho_k(r)dr = 1$ when $k = j$ and 0 otherwise. For more rapidly decaying isostable coordiantes, no constructive definition can be written, rather, these isostable coordinates can be thought of as level sets of Koopman eigenfunctions [21]. Note that these isostable coordinates are defined in the entire basin of attraction of the stationary solution. The relationship between isostable coordinates and level sets of the Koopman operator was highlighted in [13].

As illustrated in [20], under the flow of (1), the isostable dynamics are simply, $d\psi_j/dt = \lambda_j\psi_j$. Furthermore, near the steady state solution, to a linear approximation, $s_j[X(r,0)-X_{\mathrm{SS}}] = \psi_j\{X(r,0)\}$. As implemented in other applications [18], [17], it is often possible to obtain a good approximation for the output by only considering the first N isostable coordinates (i.e., truncating the rapidly decaying components of the transient solution). By letting $y(t)$ and $C_d(\rho_j)$ represent discretized versions of the solution output $\equiv Y(r,t)-Y_{SS}(r)$ and $C(\rho_j)$, respectively, in column vector format and assuming that $y(t)$ is small, then to leading order accuracy

$$\begin{aligned} y(t) &\approx \sum_{j=1}^{N}\psi_j C_d(\rho_j), \\ &= P\Psi(t), \end{aligned} \quad (5)$$

where $\Psi(t) = \begin{bmatrix}\psi_1(t) & \dots & \psi_N(t)\end{bmatrix}^T$ and $P = \begin{bmatrix}C_d(\rho_1) & \dots & C_d(\rho_N)\end{bmatrix}$. The POD framework [1] can also be used to represent the outputs as

$$y(t) \approx \sum_{j=1}^{N_p}\phi_j\mu_j(t) = \Phi M(t), \quad (6)$$

where $\phi_1,\dots,\phi_{N_p}$ are a set of orthogonal POD modes (stacked as column vectors), μ_j are associated coefficients, N_p is the number of modes required to capture the desired amount of energy, $M(t) = \begin{bmatrix}\mu_1(t) & \dots & \mu_{N_p}(t)\end{bmatrix}$, and Φ is a matrix comprised of each of the POD modes. Assuming the columns of P are linearly independent, and drawing on the orthogonality of the modes comprising Φ, Equations (5) and (6) can be manipulated to yield $\Psi = P^\dagger\Phi M$ and $M = \Phi^T P\Psi$, where † and ^{T} indicate the pseudoinverse and transpose, respectively. This implies

$$\begin{aligned} \dot{M} &= \Phi^T P\dot{\Psi} \\ &= \Phi^T P\Lambda\Psi \\ &= \Phi^T P\Lambda P^\dagger\Phi M = A_\mu M. \end{aligned} \quad (7)$$

where in the second line, the relationship $\dot{\Psi} = \Lambda\Psi$ is used where Λ is a diagonal matrix comprised of eigenvalues λ_j associated with the isostable coordinates, and $A_\mu \equiv \Phi^T P\Lambda P^\dagger\Phi$. Using standard techniques one can write $A_\mu = W\Sigma W^{-1}$ where Σ is in the Jordan normal form. Similar to the approach illustrated in [22], taking λ_j^D be the j^{th} element on the diagonal of Σ, one can define a so called "data-driven" isostable model of the form

$$\begin{aligned} \dot{\psi}_j^D &= \lambda_j^D\psi_j^D, \\ y(t) &= \sum_{k=1}^{N_p}\Upsilon_k\psi_k^D, \end{aligned} \quad (8)$$

for $j = 1,\dots,N_p$. Above Υ_k is the mode associated with ψ_k^D and is given by the k^{th} column of ΦW, and ψ_j^D is a data-driven isostable coordinate (with similar dynamics to standard isostable coordinates). Furthermore, each ψ_j^D coordinate can be inferred directly from the state according to $\psi_j^D = e_j^T W^{-1}\Phi^T$ where e_j is the j^{th} element of the standard unit basis.

In experiments, in order to extract isostable modes from the flow data, it is explicitly assumed that $b_{\mathrm{t}}(r,t)$ from (2) is responsible for statistical fluctuations observed in the data and acts to continually excite the system, keeping it from reaching its steady equilibrium. In this case, the underlying isostable coordinates themselves will not perfectly follow $\dot{\psi}_j^D = \lambda_j^D\psi_j^D$, however, provided $b_{\mathrm{t}}(r,t)$ is small in magnitude one can still obtain an estimate of A_μ from the experimental data from the slowly decaying modes. Isostable modes are extracted from experimental imaging data using the following procedure: **1)** POD is performed on the data, 9 POD modes are used to determine a basis for the data. **2)** At $\Delta t = 100$ microsecond intervals, coefficients of the POD basis are calculated according to $M(t) = \Phi^T y(t)$, a least squares fitting strategy is used to find the elements of the matrix A which best captures the relationship

$$\mu(t+\Delta t) = A\mu(t). \quad (9)$$

This is accomplished as in [22] by taking $\zeta = 2501$ measurements equally spaced in time, defining two different matrices $B_1 = \begin{bmatrix}\mu(0) & \mu(\Delta t) & \dots & \mu((\zeta-1)\Delta t)\end{bmatrix}$, $B_2 = \begin{bmatrix}\mu(\Delta t) & \mu(2\Delta t) & \dots & \mu(\zeta\Delta t)\end{bmatrix}$ and taking $A = B_1^\dagger B_2$. **3)** The matrices A_μ from Equation (7) and A from Equation (9) describe continuous time behavior and discrete time relationships for the same system, respectively. The eigenvalues of A_μ and A (λ_j^D and λ_j^A, respectively) are related by $\lambda_j^D = \log(\lambda_j^A)/\Delta t$. Eigenvectors of A and A_μ are identical.

This reduction strategy is applied to the hypersonic flow data, and a subset of the resulting modes are shown in Figure 2. The modes shown in panels B-D are associated with the largest average square of the corresponding isostable coordinate, $\frac{1}{T_{\mathrm{r}}}\int_0^{T_{\mathrm{r}}}\psi_j^D\psi_j^{D*}dt$ where * denotes the complex conjugate and T_{r} is the duration of the experiment. Panel A shows the average measured value of the experimental data which is taken to be Y_{SS}. The first mode in panel B is strictly real and captures the boundary layer on the flat plate. The negative amplitude regions correspond to the regions where the forward lambda-shock foot oscillates. The second mode is complex corresponding to an exponentially decaying sinusoid with an associated frequency of $\mathrm{Imag}(\lambda_2^D)/2\pi = 4.73$

kHz. This mode characterizes the oscillations in the lambda-shock structure. Interestingly, this frequency corresponds exactly to the peaks in the power spectrum observed in [16] using techniques involving Fourier transformations applied to the same dataset. Using (8) with only the three modes shown in panels B-D of Figure 2 can be used to qualitatively replicate the unsteady dynamical behavior of observed in experimental data.

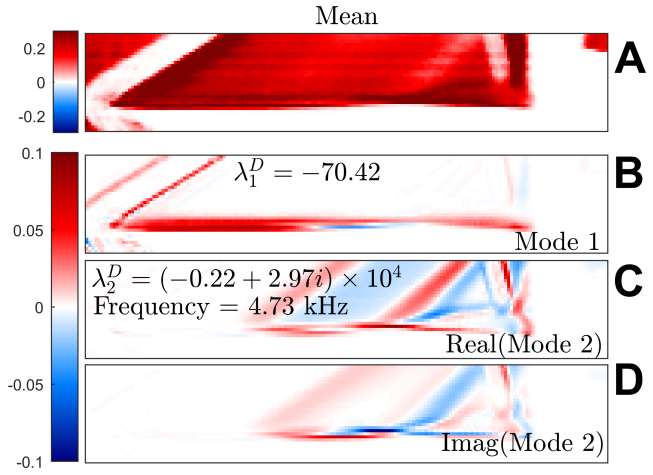

Fig. 2. Panel A shows the average of the imaging data taken over the course of the experiment. Two modes obtained using isostable methods are also shown. In panel B, a strictly real mode which captures the boundary layer region and lambda-shock foot oscillation region is shown. Panels C and D show real and imaginary components, respectively, of a mode that characterizes oscillations in the lambda-shock structure.

IV. Comparison to Well-Established Strategies

Here we investigate the same dataset using other well-established model reduction strategies including POD and spectral POD. We emphasize that while the data-driven isostable reduced framework above uses POD as a starting point, POD alone does not contain underlying information about the dynamical behavior.

A. Image Analysis Based on POD

We now compare the isostable reduction method to more well-established reduction frameworks. Proper orthogonal decomposition (POD), introduced by [23] and detailed by [24] is an efficient model reduction technique used to reduce nonlinear infinite dimensional systems to lower order finite dimensional systems, especially those that describe the dynamics of fluid flows. POD has increasingly been used recently as a model order reduction technique to achieve faster simulations of complicated high-dimensional systems. POD models of only a few dozen states have been shown to accurately capture the system dynamics of the full order system model of thousands of states [25]. POD provides an optimal set of orthogonal basis functions, which when visualized, shows the coherent structures of the system dynamics over the spacial domain. Given a function $w(x,t)$ in the standard Hilbert space $L^2(\Omega,T)$ where $x \in \Omega$ for some $\Omega \subset \mathbb{R}^p$ and T is a finite time interval. The n POD basis functions set $\{\phi_i\}_{i=1}^n$ is computed by minimizing the following cost function:

$$J(\phi) := \int_0^T \int_\Omega |w(x,t) - \sum_{i=1}^n \alpha_i(t)\phi_i(x)|^2 dxdt, \tag{10}$$

where $w(x,t)$ is the solution of the governing PDE which is usually difficult to analytically compute and α_i is the temporal coefficient of each basis function. Alternatively, numerical simulations are easier to compute and the solution is defined at the mesh locations at different times (snapshots) $\{s_i\}_{i=1}^N$, then the optimization problem becomes discrete as follows:

$$J(\phi) := \sum_k \sum_m |s(x_m,t_k) - \sum_{i=1}^n \alpha_i(t_k)\phi_i(x_m)|^2. \tag{11}$$

For a given snapshots matrix s, the solution of the optimization problem (11) up to n pod basis functions is given by the n eigenvectors corresponding to the largest n eigenvalues of the eigenvalue problem [24]:

$$ss^T\phi = \lambda\phi. \tag{12}$$

Figure 3 shows the dominant POD modes ranked by preserved energy in descending order for the supersonic flow data.

B. Image Analysis Based on Spectral POD

Snapshot-based POD does not explicitly contain any information about the frequency content of each mode. Some frequency content can be revealed by computing the power spectrum of each each $\alpha_i(t)$ (as shown in Figure 4), however, this by itself will not give a full picture of the spatiotemporal behavior. Such information can be gained by using spectral POD (SPOD) analysis [5] which considers the frequency domain form of POD. SPOD is derived from a space-time POD problem for statistically stationary flows and leads to modes that each oscillate at a single frequency. SPOD modes represent structures that evolve coherently in space and time while POD modes in general give space-only coherent structures.

Let $w(x,t) \overset{\mathscr{F}}{\longleftrightarrow} W(x,f)$ be the Fourier transform pair defined as:

$$w(x,t) = \int_{-\infty}^{\infty} W(x,f)e^{j2\pi ft} df, \tag{13}$$

$$W(x,f) = \int_{-\infty}^{\infty} w(x,t)e^{-j2\pi ft} dt, \tag{14}$$

The n SPOD basis functions set $\{\psi_i\}_{i=1}^n$ is computed by minimizing the following cost function:

$$J(\psi) := \int_0^T \int_\Omega |W(x,f) - \sum_{i=1}^n F_i(f)\psi_i(x)|^2 dxdt, \tag{15}$$

where ψ is the spectral modes and F is the frequency coefficients. The discrete form is:

$$J(\psi) := \sum_k \sum_m |S(x_m,f_k) - \sum_{i=1}^n F_i(f_k)\psi_i(x_m)|^2. \tag{16}$$

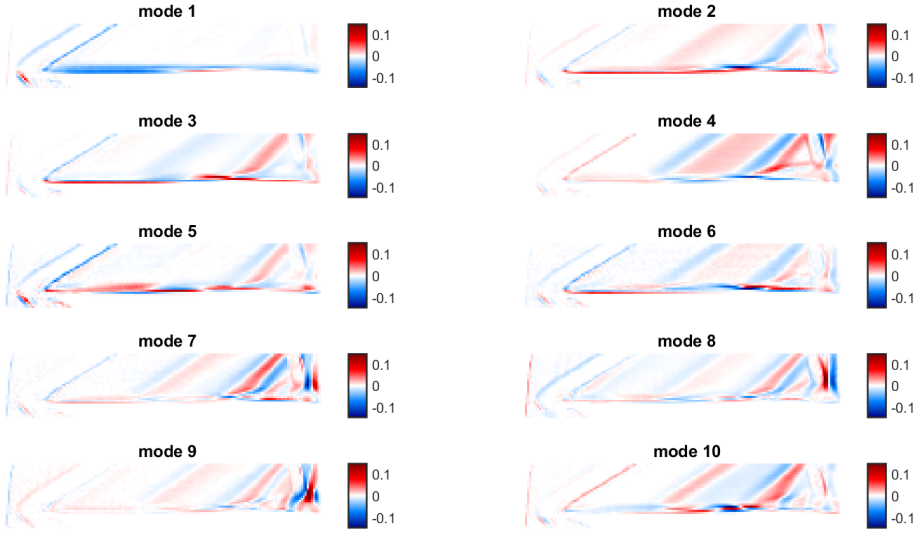

Fig. 3. Dominant POD modes ranked by the preserved energy in descending order. In each mode the lambda-shock structure can be observed, however, it is not possible to identify the temporal characteristics of the flow using POD alone.

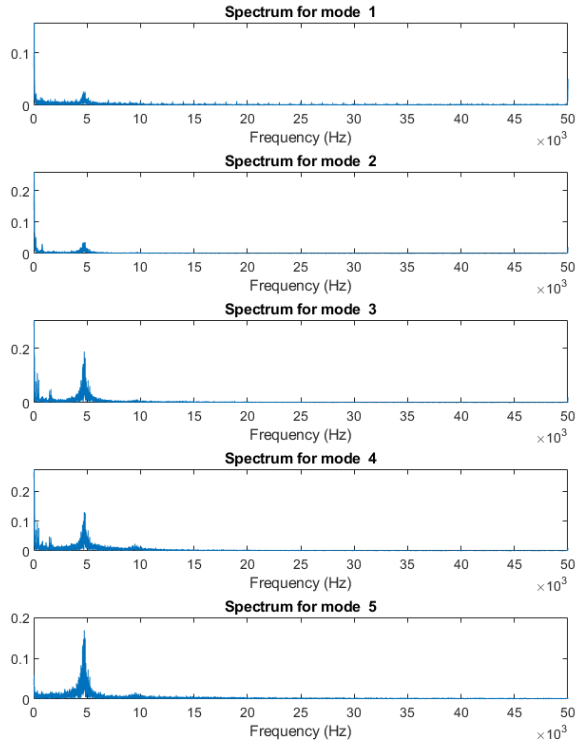

Fig. 4. POD temporal coefficients and their frequency spectrum. Each of the modes has significant frequency content near 4.7 kHz.

The solution is given by the n eigenvectors that correspond to the maximum n eigenvalues in the eigenvalue problem:

$$SS^T\psi = \lambda\psi, \tag{17}$$

where $s(x_m,t_k) \overset{\mathscr{F}}{\longleftrightarrow} S(x_m,f_k)$. Real and Imaginary parts of the first 5 SPOD modes at 4.7 kHz are shown in Figure 5.

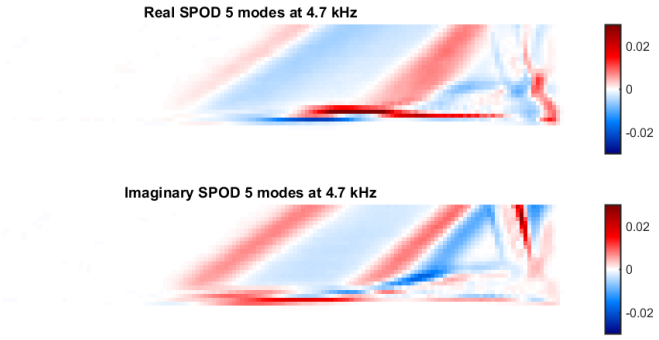

Fig. 5. Real and Imaginary parts of the first 5 SPOD modes at 4.7 kHz. Similar features are observed as compared to the isostable reduction methodology from Section III even though the two modes are obtained through fundamentally different approaches.

C. Image Analysis Based on DMD

Image analysis using DMD was performed on similar experimental datasets in [26] and is not repeated here. The DMD framework was able to identify modes that correspond to shock breathing when considering experimental setups with both turbulent and transitional boundary layers. As with most applications of DMD applied to experimental data, the authors of [26] remark that because DMD analysis outputs a large number of modes and that the modes are not sorted by order of importance it somewhat subjective to identify which modes are worth investigating.

V. Conclusion

In this work, a strategy is developed for identifying a first order accurate isostable reduced model from noisy experimental data. This strategy is applied to analyze the unsteady, temporal characteristics of cylinder-generated shock-wave/transitional boundary-layer interaction resulting from Mach 2 flow. Using this approach, the temporal behavior is

well-characterized with a pair of complex-conjugate isostable coordinates that are driven by exogenous input. This approach identifies two modes that correspond to exponentially decaying sinusoids with frequency 4.73 kHz. For this same dataset, this frequency corresponded to peaks found in the power spectrum of the imaging data [16], and also coincided with the dominant frequency in the spectral POD strategy shown here.

It is notable that the imaginary mode shapes from panel C and D of Figure 2 are very similar to those observed in Figure 5 despite the fact that the two methods approach the reduction from a different perspective, with the former identifying a dynamical model for the most important mode shapes and the latter attempting to identify dominant modes that characterize the data across both space and time. It is feasible that there could be an unexplored connection between both of these reduction strategies, especially when considering the reduced isostable framework in the vicinity of a stationary solution so that linearization is possible.

The methodology described in Section III gives a linear approximation of the isostable mode shapes for use when the dynamics are close to a stationary solution. It may be possible to develop strategies to provide higher order accurate approximations for the model dynamics similar to the strategy suggested in [17]. Additionally, given that isostable coordinates are valid in the entire basin of attraction of a limit cycle, it may be possible to characterize the behavior along trajectories for initial conditions that have been perturbed farther from the stationary solution. Finally, it would be of interest to incorporate the influence of perturbations into the reduced model dynamics from (8) using a 'direct method' that characterizes the influence of spatiotemporal perturbations (i.e., pulsed jet injection upstream of the shock interaction region) on the reduced isostable coordinates after the rapidly decaying transients have died out. Such strategies would allow for active control strategies to be implemented in experiments even when a full dynamical description (based on the Navier-Stokes equations) is unavailable. Such considerations will be investigated in future studies.

ACKNOWLEDGMENT

This material is based upon research supported by the U.S. Office of Naval Research under award number N00014-15-1-2269 and by the National Science Foundation under award number CMMI-1933583.

REFERENCES

[1] P. Holmes, J. L. Lumley, G. Berkooz, and C. W. Rowley, *Turbulence, Coherent Structures, Dynamical Systems and Symmetry*. New York: Cambridge University Press, 1996.

[2] K. Taira, S. L. Brunton, S. T. M. Dawson, C. W. Rowley, T. Colonius, B. J. McKeon, O. T. Schmidt, S. Gordeyev, V. Theofilis, and L. S. Ukeiley, "Modal analysis of fluid flows: an overview," *AIAA Journal*, pp. 4013–4041, 2017.

[3] G. Berkooz, P. Holmes, and J. L. Lumley, "The proper orthogonal decomposition in the analysis of turbulent flows," *Annual Review of Fluid Mechanics*, vol. 25, no. 1, pp. 539–575, 1993.

[4] S. Sahyoun and S. M. Djouadi, "Time, space, and space-time hybrid custering pod with application to the burgers' equation," in *53rd IEEE Conference on Decision and Control*. IEEE, 2014, pp. 2088–2093.

[5] A. Towne, O. T. Schmidt, and T. Colonius, "Spectral proper orthogonal decomposition and its relationship to dynamic mode decomposition and resolvent analysis," *Journal of Fluid Mechanics*, vol. 847, p. 821867, 2018.

[6] C. W. Rowley and S. T. M. Dawson, "Model reduction for flow analysis and control," *Annual Review of Fluid Mechanics*, vol. 49, pp. 387–417, 2017.

[7] A. Varshney, S. Pitchaiah, and A. Armaou, "Feedback control of dissipative PDE systems using adaptive model reduction," *AIChE Journal*, vol. 55, no. 4, pp. 906–918, 2009.

[8] P. J. Schmid, "Dynamic mode decomposition of numerical and experimental data," *Journal of Fluid Mechanics*, vol. 656, pp. 5–28, 2010.

[9] I. Mezić, "Analysis of fluid flows via spectral properties of the Koopman operator," *Annual Review of Fluid Mechanics*, vol. 45, pp. 357–378, 2013.

[10] M. Budišić, R. Mohr, and I. Mezić, "Applied Koopmanism," *Chaos: An Interdisciplinary Journal of Nonlinear Science*, vol. 22, no. 4, p. 047510, 2012.

[11] S. L. Brunton, J. L. Proctor, and J. N. Kutz, "Discovering governing equations from data by sparse identification of nonlinear dynamical systems," *Proceedings of the National Academy of Sciences*, vol. 113, no. 15, pp. 3932–3937, 2016.

[12] H. Arbabi and I. Mezic, "Ergodic theory, dynamic mode decomposition, and computation of spectral properties of the Koopman operator," *SIAM Journal on Applied Dynamical Systems*, vol. 16, no. 4, pp. 2096–2126, 2017.

[13] A. Mauroy, I. Mezić, and J. Moehlis, "Isostables, isochrons, and Koopman spectrum for the action–angle representation of stable fixed point dynamics," *Physica D: Nonlinear Phenomena*, vol. 261, pp. 19–30, 2013.

[14] D. S. Dolling, "Fluctuating loads in shock wave/turbulent boundary layer interaction: tutorial and update," in *31st Aerospace Sciences Meeting*, 1993, p. 284.

[15] D. D. Knight and G. Degrez, "Shock wave boundary layer interactions in high Mach number flows. a critical survey of current numerical prediction capabilities," Advisory Group for Aerospace Research and Development Report, no. 319, 1998.

[16] C. S. Combs, L. E. Lash, P. A. Kreth, and J. D. Schmisseur, "Investigating unsteady dynamics of cylinder-induced shock-wave/transitional boundary-layer interactions," *AIAA Journal*, vol. 56, no. 4, pp. 1588–1599, 2018.

[17] D. Wilson and B. Ermentrout, "Greater accuracy and broadened applicability of phase reduction using isostable coordinates," *Journal of Mathematical Biology*, vol. 76, no. 1-2, pp. 37–66, 2018.

[18] ——, "Augmented phase reduction of (not so) weakly perturbed coupled oscillators," *SIAM Review*, vol. 61, no. 2, pp. 277–315, 2019.

[19] D. Wilson and S. Djouadi, "Isostable reduction and boundary feedback control for nonlinear convective flow," in To Appear in *Preceedings of the 58th IEEE Conference on Decision and Control*.

[20] D. Wilson and J. Moehlis, "Isostable reduction with applications to time-dependent partial differential equations," *Physical Review E*, vol. 94, no. 1, p. 012211, 2016.

[21] I. Mezić, "Spectrum of the Koopman operator, spectral expansions in functional spaces, and state-space geometry," *Journal of Nonlinear Science*, pp. 1–55, 2019.

[22] D. Wilson, "A data-driven phase and isostable reduced modeling framework for oscillatory dynamical systems," *Chaos: An Interdisciplinary Journal of Nonlinear Science*, vol. 30, no. 1, p. 013121, 2020.

[23] J. Lumley, *Stochastic Tools in Turbulence*. New York Academic Press, 1970.

[24] P. Holmes, J. Lumley, and G. Berkooz, *Turbulence, Coherent Structures, Dynamical Systems and Symmetry*, ser. Cambridge Monographs on Mechanics. Cambridge University Press, 1998. [Online]. Available: https://books.google.com/books?id=7vS1nPYDe10C

[25] S. M. Djouadi, R. C. Camphouse, and J. H. Myatt, "Reduced order models for boundary feedback flow control," in *2008 American Control Conference*, June 2008, pp. 4005–4010.

[26] C. S. Combs, J. D. Schmisseur, B. F. Bathel, and S. B. Jones, "Analysis of shock-wave/boundary-layer interaction experiments at mach 1.8 and mach 4.2," in *AIAA Scitech 2019 Forum*, 2019, p. 0344.